ACS Photonics

pubs.acs.org/journal/apchd5

Article

Nanolaser Using Colloidal Quantum Wells Deterministically Integrated on a Nanocavity

David Sharp, Ruiming Lin, Hao Nguyen, Arnab Manna, Hannah Rarick, Christopher Munley, Wooje Cho, Dmitri Talapin, Brandi Cossairt, and Arka Majumdar*

Cite This: https://doi.org/10.1021/acsphotonics.4c00377

Read Online

ACCESS | Metrics & More | Article Recommendations

ABSTRACT: On-chip light sources based on hybrid integration of colloidal semiconductor nanocrystal emitters with integrated photonics have focused on either colloidal emitters ill-suited to act as gain media due to large Auger recombination or nonscalable suspended nanocavity geometries with a randomly positioned colloidal gain material. In this work, we demonstrate a nanolaser by integrating colloidal quantum wells with an on-substrate nanobeam cavity geometry. We employ deterministic positioning of colloidal quantum wells to enhance the coupling of the gain material to the cavity. This device achieves lasing under continuous-wave optical pumping at room temperature with a threshold of 2.9 μW, which demonstrates the suitability of this hybrid platform for scalable on-chip light sources. Additionally, we show that the shelling of the colloidal quantum wells is essential for maximizing gain.

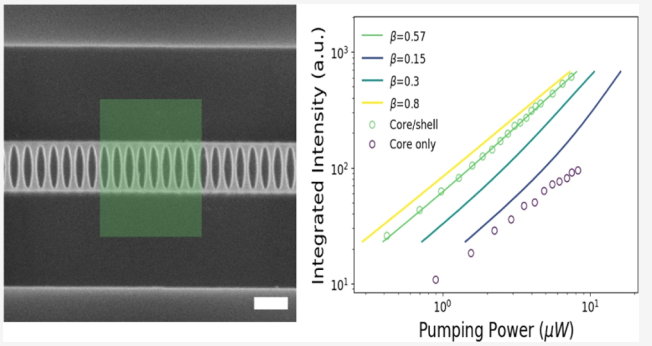

KEYWORDS: *colloidal nanocrystal, colloidal quantum well, nanolaser, cavity, integrated photonics*

INTRODUCTION

Hybrid integration of photonic devices with colloidal semiconductor nanocrystals is a compelling route toward large-scale active photonic devices that leverage the scalability of both complementary metal-oxide-semiconductor (CMOS)-compatible photonic platforms and inexpensive colloidal nanocrystal synthesis techniques. In particular, on-chip nanolasers are an attractive application of hybrid integration that combines gain media with low-loss dielectric nanophotonic structures.[1] Colloidal semiconductor nanocrystals themselves have shown promise as a gain material in which a nanolaser is formed by self-assembly of the colloidal material into geometries, such as whispering gallery mode resonators[2−4] and microdisks.[5] However, these self-assembled geometries are not appropriate for large-scale applications due to their fabrication disorders and CMOS incompatibility. Recent effort has instead turned to hybrid integration of colloidal semiconductor nanocrystals, including II−VI colloidal quantum dots (cQDs),[6] perovskite cQDs,[7] and II−VI colloidal quantum wells (cQWs), also known as colloidal nanoplatelets,[8] with nanobeam photonic crystal cavities. As compared to hybrid integration efforts with other geometries, such as distributed Bragg reflector cavities[9] and Fabry−Pérot cavities,[10] nanobeam cavities have a small mode volume that tightly localizes the cavity mode and enhances the light−matter coupling strength.

CdSe/CdS cQWs are a promising candidate for the colloidal nanocrystal gain material because their reduced Auger recombination rate, compared to II−VI cQDs, enables high gain[11,12] and lasing when integrated with a suspended silicon nitride (SiN) nanobeam cavity geometry.[8] Unfortunately, the fragile nature of the suspended geometry precludes both scalability and the ability to position the gained material selectively and deterministically on the cavity. On-substrate SiN nanobeam cavities with improved thermal and mechanical stability address this pitfall and have been used successfully to create nanolasers with hybrid integration of perovskite cQDs without deterministic positioning.[13] As an overview of the cQW-nanobeam cavity system used herein, Figure 1a,b depicts the absorption/photoluminescence (PL) spectra and a representative transmission electron micrograph, respectively, of the cQWs used in this work, and Figure 1c depicts a scanning electron micrograph of a typical nanobeam cavity. We used an on-substrate SiN nanobeam photonic crystal cavity with deterministic positioning of cQWs to selectively couple

Received: March 1, 2024
Revised: April 15, 2024
Accepted: April 23, 2024

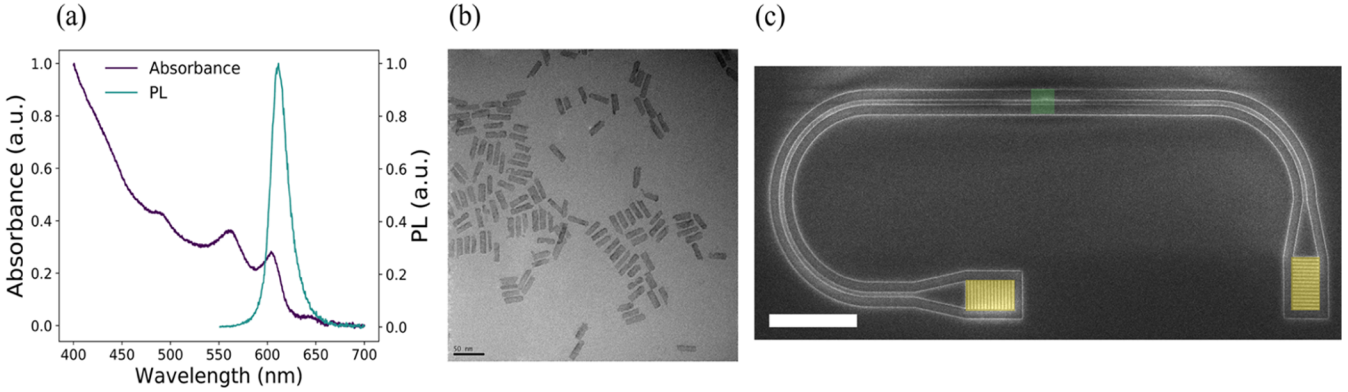

Figure 1. Overview of the nanolaser. (a) Absorption and PL spectra of CdSe/CdS cQWs. (b) Transmission electron micrographs of CdSe/CdS cQWs. The scale bar is 50 nm. (c) Scanning electron micrograph of an example SiN nanobeam cavity. The cavity region coupled to cQWs and the grating couplers for collecting cavity-coupled cQW photoluminescence are highlighted in green and yellow, respectively. The scale bar is 10 μm.

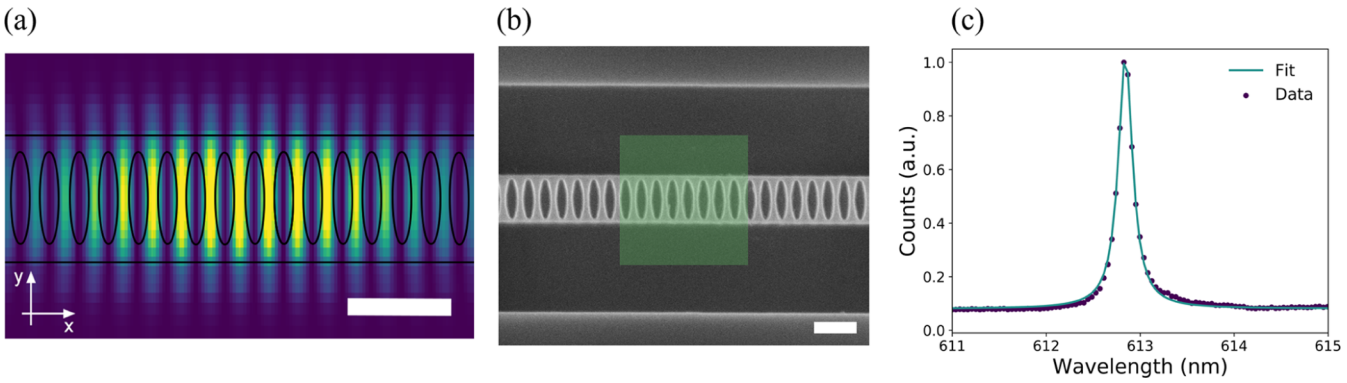

Figure 2. Design, fabrication, and characterization of the SiN nanobeam cavity. (a) The profile of the cavity mode electric field E_y from the FDTD simulation. The scale bar is 500 nm. (b) Scanning electron micrograph of the nanobeam cavity defect region. The PMMA window is highlighted in green. The scale bar is 500 nm. (c) Nanobeam cavity transmission spectrum as measured by sending a broadband laser through the grating couplers without cQWs coupled to the cavity. The lowest-order transverse electric (TE) cavity mode is evidenced by a Lorentzian peak with a quality factor of ~2400.

the gain material to the cavity. By utilizing a hybrid integration scheme, we demonstrated a nanolaser with an amplified spontaneous emission threshold of 2.9 μW under continuous wave pumping and found that cQW shelling is essential to maximizing gain. Such control of the colloidal gain material has not yet been exploited for nanolasers and represents a step forward for scalable on-chip light sources.

METHODS

Four mL CdSe cQWs were synthesized according to previous literature.[14] Briefly, 170 mg of cadmium myristate, 12 mg of selenium powder, and 15 mL of octadecene (ODE) were combined in a 50 mL three-neck flask and evacuated at room temperature for 1 h. Under nitrogen flow, the flask was heated to 240 °C. At 190 °C, 40 mg of finely ground cadmium acetate dihydrate was quickly added to the flask. The reaction temperature was maintained for 10 min after reaching 240 °C and then quickly cooled by air flow. At 100 °C, a solution of 2 mL of oleic acid in 15 mL of methylcyclohexane (MCH) was injected, and the solution was stirred under nitrogen overnight. The cQWs were isolated by centrifugation at 11,000 rpm for 10 min. The pellets were redispersed in MCH.

Subsequently, CdS shell growth was performed on 4 mL CdSe cQWs by colloidal atomic layer deposition (c-ALD) based on literature methods.[15] In a nitrogen-filled glovebox, core cQWs (~20 mg) were precipitated from the stock solution in MCH with ethanol. The cQWs were redispersed in 100 μL of MCH and combined in a 4 mL vial with 500 μL of ODE, 100 μL of oleylamine, and 10 mg of Li_2S with a glass stir bar. The mixture was stirred at 150 °C on a hot plate for 90 s. The S^{2-}-capped cQWs were precipitated once with ethanol and then redispersed in 100 μL of MCH. To grow the Cd layer, the cQW solution was added to a 4 mL vial containing 500 μL of ODE, 100 μL of oleylamine, and 15 mg of cadmium formate. The mixture was stirred at 150 °C for 3 min, followed by centrifugation and decantation to remove excess solids. The cQWs were precipitated with ethanol and redispersed in 100 μL of MCH. This completed one monolayer growth of CdS shell. The second monolayer was grown by repeating the same process.

The nanobeam cavity was designed for thin-film SiN on buffer SiO_2 with poly(methyl methacrylate) (PMMA) encapsulation. The refractive index of PMMA closely matches that of the underlying SiO_2, which preserves the out-of-plane inversion symmetry.[16] This has been shown to enable high-quality-factor SiN nanobeam cavity designs.[17,18] Verification of the cavity design was implemented in the finite-difference time-domain (FDTD) solver from Lumerical. The simulation layout consisted of a SiN waveguide with elliptical holes surrounded by a uniform PMMA/SiO_2 medium. The 220 nm thick SiN waveguide was set to an unperturbed elliptical hole period of 183 nm, a defect period of 175 nm, an elliptical hole

https://doi.org/10.1021/acsphotonics.4c00377
ACS Photonics XXXX, XXX, XXX−XXX

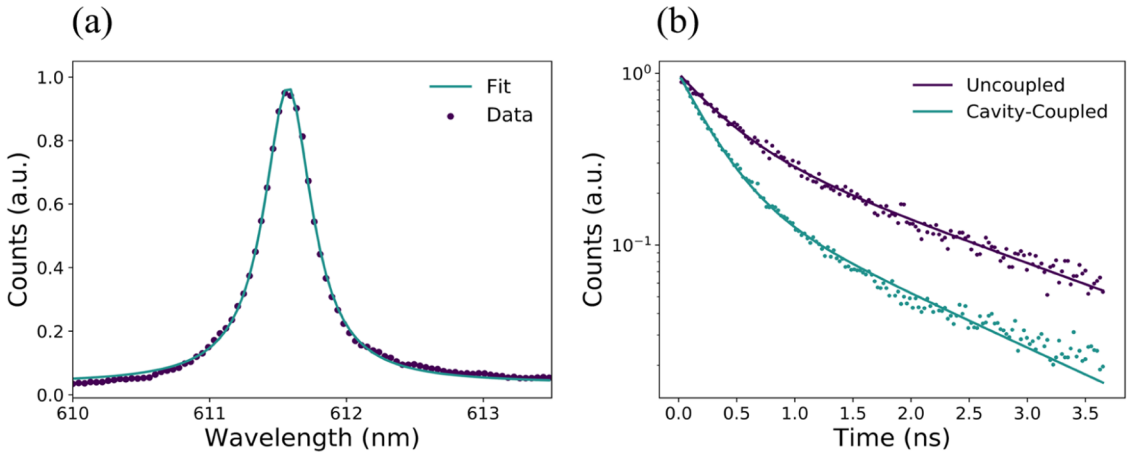

Figure 3. Characterization of the cavity-coupled cQWs. (a) The cavity-PL spectrum as measured by optically pumping the cQW PL and collecting through a grating coupler. The same cavity mode is presented. (b) Time-resolved PL data for both uncoupled and cavity-coupled cQWs. The solid lines represent biexponential decay fits for each data set.

major radius of 220 nm, a minor radius of 50 nm, and a waveguide width of 550 nm. The cavity defect was formed in the center by quadratically tapering the elliptical hole periodicity from the defect period to the unperturbed period over 10 periods on either side. Extra mirrors to strengthen the light confinement were formed by adding 15 more periods of unperturbed elliptical holes on either end. The resulting cavity mode electric field profile is shown in Figure 2a. This resulted in a theoretical quality of a factor of ∼10,000 and a mode volume of ∼2.1 $(\lambda/n)^3$.

The nanobeam cavity was fabricated using a 220 nm thick LPCVD SiN on 4 μm thermal SiO_2 on a silicon wafer from Rogue Valley Microdevices. To define the pattern, ∼300 nm thick ZEP520A positive-tone electron-beam lithography resist was spun-coated on the surface and patterned with a 100 kV electron-beam lithography system. The pattern was transferred to the underlying SiN layer using a plasma etch consisting of fluorine-based chemistry. Figure 2b shows a scanning electron micrograph of the nanobeam cavity centered on the defect region. In order to deterministically position ensembles of cQWs on the nanobeam cavities, windows in a cladding layer of PMMA were opened with a subsequent aligned electron-beam lithography step. This has been shown to increase the coupling efficacy of colloidal nanocrystals to nanobeam cavities by ensuring that the cQWs pack into a thick film on top of the nanobeam cavity.[6]

RESULTS AND DISCUSSION

Before integrating the cQWs, the nanobeam cavities were first characterized using transmission measurements since the nanobeam cavity is coupled to a SiN waveguide and grating couplers. A broadband laser was shined on one grating coupler, and the transmission spectrum was collected at the other grating coupler using a confocal multimode optical fiber. Figure 2c shows an example transmission spectrum of a nanobeam cavity. Although several modes are present, the results here focus on the coupling of the lowest-order TE mode. By fitting to a Lorentzian line shape, the experimental quality factor is found to be ∼2400. The experimental quality factor is smaller than the simulated quality factor, which is attributed to fabrication imperfections.

cQWs were integrated with the nanobeam cavities by drop-casting a hexane solution containing cQWs onto a chip containing many nanobeam cavities prepared with open PMMA windows. The devices were re-encapsulated with PMMA to cover the open windows. This enhances the cQW-cavity coupling and reduces the scattering of light in the waveguide from uncoupled cQWs. Both effects maximize the signal-to-noise ratio of cavity-coupled photoluminescence (cavity-PL) relative to uncoupled background PL. The coupling of cQWs was first confirmed by measuring the cavity-PL spectrum. For all cavity-PL experiments, the chip was placed in a vacuum chamber to prevent the degradation of the cQWs under laser excitation. A 445 nm continuous wave pump laser was shined on the cavity defect region containing cQWs by using a 40× (0.6 NA) objective lens, and the cavity-PL spectrum was collected at a grating coupler to minimize background from uncoupled cQWs. The cavity-PL spectrum for the nanobeam cavity considered in the rest of this work is shown in Figure 3a. By fitting this spectrum to a Lorentzian line shape at high pump powers, a cQW-cavity-coupled quality factor of ∼830 is extracted. The degradation of the pristine nanobeam cavity quality factor indicates that the cQWs are coupled well to the cavity.[6] Coupling of cQWs can introduce TE/TM mode splitting via out-of-plane refractive index symmetry breaking, but only the fundamental TE mode was observed in the cavity-PL spectrum.

Time-resolved measurements of the cavity-PL were performed to further confirm the coupling of the cQWs to the nanobeam cavities because it is expected that the nanobeam cavities will reduce the cQW spontaneous emission lifetime by the Purcell enhancement factor.[19] In the limit where the emitter line width is much broader than the cavity line width, this factor is given by[8]

$$F_p = 1 + \frac{3\lambda^3 Q_{em}}{4\pi^2 n^3 V}\psi(r) \quad (1)$$

where λ is the cavity resonance wavelength, Q_{em} is the quality factor of the cQW PL, n is the refractive index of the cavity dielectric, V is the cavity mode volume, and $\psi(r)$ is the ratio of the cavity mode electric field intensity at the emitter's location to the global maximum. For this system, $Q_{em} \sim 34$ and $\psi(r)$ is 0.32 as the cQWs interact with the evanescent field on top of the nanobeam cavity. Therefore, the theoretical Purcell enhancement F_p is ∼1.4.

https://doi.org/10.1021/acsphotonics.4c00377
ACS Photonics XXXX, XXX, XXX−XXX

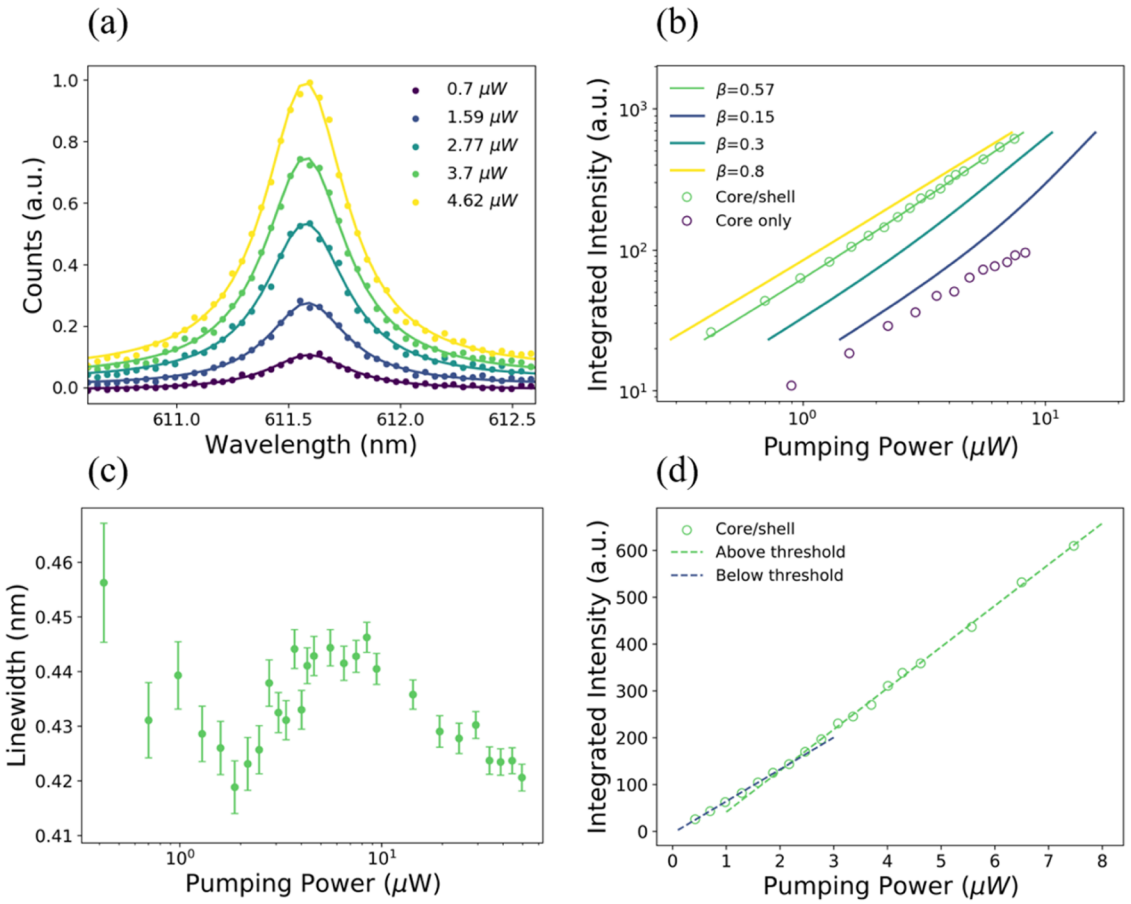

Figure 4. Characterization of lasing in the cQW-nanobeam cavity system. (a) Pumping-power-dependent cavity-PL spectra. The solid lines represent Lorentzian fittings to the cavity modes at each pumping power. The cavity mode peak emerges as the pumping power surpasses the amplified spontaneous emission threshold near 2.9 μW. (b) The dependence of the area under the cavity mode peak as a function of pumping power plotted on a log−log scale. The curve has a soft kink at the pumping power threshold, which is indicative of high-β lasing. Plots of the solution to the laser rate equation with other values for β and experimental data for core-only cQWs coupled to a similar nanobeam cavity are both shown. (c) The line width of the cavity mode peak as a function of pumping power from fitting to a Lorentzian line shape plotted on a linear-log scale. Above the threshold, the line width decreases as a function of pumping power. The error bars represent the curve fitting error. (d) The same core/shell cQW data as shown in (b) with linear fits above and below the threshold plotted on a linear−linear scale.

The time-resolved PL was collected for both uncoupled and cavity-coupled cQWs using a pulsed pump laser (532 nm, 80 MHz repetition rate) and is shown in Figure 3b. The lifetime was extracted by fitting the time-resolved PL to a biexpontential decay model due to the presence of two radiative decay pathways in CdSe/CdS cQWs.[20] From these fits, fast and slow decay time constants 0.39 and 1.77 ns (0.27 and 1.39 ns), respectively, were extracted for uncoupled (cavity-coupled) cQWs. This corresponds to an average Purcell enhancement of 1.3, which is slightly smaller than the theoretical prediction because not all of the cQWs are coupled to the cavity mode electric field maximum.

To characterize the lasing behavior of the nanobeam cavity coupled to cQWs, power-dependent cavity-PL measurements were performed. The pumping power was monitored by a beam splitter in front of the objective lens, and cavity-PL spectra were recorded at each pumping power. Figure 4a depicts the cavity-PL spectra collected at different pumping powers. This shows an evolution of the cavity mode from a weak mode dominated by the background uncoupled cQW PL to a clear cavity peak as the system transitions to an amplified spontaneous emission regime.

Figure 4b,d shows the "light in−light out" curve, i.e., the dependence of the cavity mode intensity, defined here as the integrated area under the cavity mode Lorentzian peak, on the pumping power, respectively, plotted on the log−log and linear−linear scale. The light-in/light-out curve in Figure 4d includes linear fits above and below the lasing threshold. These data were fitted to the laser rate equation:[21]

$$R_{ex} = \frac{P}{\Gamma t_c(1 + aP)}\left(\frac{1}{\beta} + aP\right) \quad (2)$$

where R_{ex} is the external pumping rate, P is the photon number in the cavity, Γ is the cavity confinement factor, t_c is the cavity lifetime, a is the efficiency of stimulated emission into the cavity mode, and β is the ratio of emission rate into the cavity mode against emission rates into all modes. The lasing pump power threshold is commonly defined as the point in which the mean cavity photon number equals unity.[22] Therefore, eq 2 predicts that the lasing threshold occurs when the product $aP = 1$. According to the fit to eq 2, the light in−light out curve displays a high β of 0.57 that results in a soft kink at the calculated pumping power threshold of 2.9 μW, which is slightly higher than similar reports,[8] but is expected for an on-substrate cavity design as compared to a suspended one. The

https://doi.org/10.1021/acsphotonics.4c00377
ACS Photonics XXXX, XXX, XXX−XXX

discrepancy is due to the decreased index contrast for a cavity surrounded by SiO_2/PMMA rather than air, which increases the cavity mode volume and decreases the light−matter coupling strength.

Figure 4b also depicts a typical light in−light out curve for CdSe core-only cQWs coupled to a similar nanobeam cavity designed for spectral overlap with CdSe core-only cQWs.[23] This curve shows weaker cQW-cavity coupling and no clear threshold, which suggests that the CdSe/CdS cQW core/shell morphology is essential for high gain. Optical gain in both core-only and core/shell cQWs originates primarily from biexcitons.[9,14] Core-only cQWs, in comparison to their core/shell counterparts, experience charge trapping that diminishes their PL quantum efficiency, broadens PL line width, and creates delayed emission due to the unpassivated Se edge sites.[24,25] In addition to their intrinsic high susceptibility to surface defects and low stability, cQWs in thin films encounter a greater effective dielectric medium, leading to decreased exciton binding energy.[26,27] This behavior results in more severe reduced radiative recombination, decreased PL quantum yield, and ultimately lower optical gain when compared with core/shell cQWs.

The dependence of the cavity mode line width as a function of pumping power was extracted by fitting each spectrum to a Lorentzian cavity mode and is shown in Figure 4c. This shows a line width of 0.458 nm at low pumping powers that narrows to 0.418 nm and rebroadens to 0.440 nm due to the gain-index coupling below the predicted threshold.[28] As the pumping power crosses the predicted threshold, the line width monotonically decreases due to increasing coherence time in the cavity and suppression of the spontaneous emission. This line width behavior, in conjunction with the light in−light out curve, confirms that the cQW-nanobeam cavity system behaves as a nanolaser. Furthermore, this lasing behavior is attributed to photon lasing only and not polariton lasing given the broad cQW line width is expected to preclude the cQW-nanobeam cavity system from entering the strong coupling regime, as has been shown in other cavities.[29,30]

CONCLUSIONS

A continuous wave optically pumped nanolaser based on hybrid integration of solution-processed CdSe/CdS core−shell cQWs and an on-substrate SiN nanobeam cavity was demonstrated. The amplified spontaneous emission onset threshold was calculated to be 2.9 μW. In particular, deterministic integration was utilized to maximize coupling of the colloidal gain material to the nanobeam cavity, and it was shown that core/shell cQWs generate greater optical gain than their core-only counterparts, enabling lasing. The wavelength range of similar devices could span the visible spectral range by controlling the cQW composition and modifying the periodicity of the nanobeam cavity elliptical holes.[23] As previously mentioned, similar nanobeam cavities integrated with core-only CdSe cQWs did not yield lasing. This suggests that the core−shell cQW morphology is essential for optical gain and that advancements in the cQW synthesis and chemical composition, for example by creating graded heterostructures, could further improve the lasing performance.[31] cQW dynamical properties that depend on shell thickness warrant further study in the context of nanolasers. Optimization of active gain area by altering the PMMA window size could improve the lasing performance in future studies.[22] Furthermore, by incorporating the nanobeam cavity with another resonator, deterministic positioning could be used to selectively apply gain material to a single cavity to module the gain−loss balance in the coupled cavity system.[32] Electrically pumped lasing of II−VI cQD light-emitting diodes has been recently demonstrated, which suggests that electrically pumped lasing with II−VI cQWs may be possible.[33]

AUTHOR INFORMATION

Corresponding Author

Arka Majumdar − *Department of Electrical and Computer Engineering, University of Washington, Seattle, Washington 98195-2500, United States*; Email: arka@uw.edu

Authors

David Sharp − *Department of Physics, University of Washington, Seattle, Washington 98195-1560, United States*; orcid.org/0000-0002-1034-8567

Ruiming Lin − *Department of Chemistry, University of Chicago, Chicago, Illinois 60637, United States*

Hao Nguyen − *Department of Chemistry, University of Washington, Seattle, Washington 98195-1700, United States*; orcid.org/0000-0001-6742-1748

Arnab Manna − *Department of Physics, University of Washington, Seattle, Washington 98195-1560, United States*; orcid.org/0009-0007-0056-9650

Hannah Rarick − *Department of Physics, University of Washington, Seattle, Washington 98195-1560, United States*

Christopher Munley − *Department of Physics, University of Washington, Seattle, Washington 98195-1560, United States*; orcid.org/0000-0001-5684-3144

Wooje Cho − *Department of Chemistry, University of Chicago, Chicago, Illinois 60637, United States*

Dmitri Talapin − *Department of Chemistry, University of Chicago, Chicago, Illinois 60637, United States*; orcid.org/0000-0002-6414-8587

Brandi Cossairt − *Department of Chemistry, University of Washington, Seattle, Washington 98195-1700, United States*; orcid.org/0000-0002-9891-3259

Complete contact information is available at: https://pubs.acs.org/10.1021/acsphotonics.4c00377

Author Contributions

D.S. fabricated the nanobeam cavities and performed all optical characterizations and data analysis under the supervision of A.M. R.L. and W.C. synthesized core/shell cQWs under the supervision of D.T. H.N. synthesized core-only cQWs under the supervision of B.C. A.M., C.M., and H.R. assisted with data analysis and discussions. All authors gave input on writing.

Funding

This material is based upon work supported by the National Science Foundation under Grant No. DMR-2019444. Part of this work was conducted at the Washington Nanofabrication Facility/Molecular Analysis Facility, a National Nanotechnology Coordinated Infrastructure (NNCI) site at the University of Washington with partial support from the National Science Foundation via awards NNCI-1542101 and NNCI-2025489.

Notes

The authors declare no competing financial interest.

REFERENCES

(1) Ma, R. M.; Oulton, R. F. Applications of nanolasers. *Nat. Nanotechnol.* **2019**, *14*, 12−22.

(2) Wang, Y.; Ta, V. D.; Leck, K. S.; Tan, B. H. I.; Wang, Z.; He, T.; Ohl, C. D.; Demir, H. V.; Sun, H. Robust Whispering-Gallery-Mode Microbubble Lasers from Colloidal Quantum Dots. *Nano Lett.* **2017**, *17*, 2640−2646.
(3) Yang, X.; Li, B. Laser Emission from Ring Resonators Formed by a Quantum-Dot-Doped Single Polymer Nanowire. *ACS Macro Lett.* **2014**, *3*, 1266−1270.
(4) Montanarella, F.; Urbonas, D.; Chadwick, L.; Moerman, P. G.; Baesjou, P. J.; Mahrt, R. F.; Van Blaaderen, A.; Stöferle, T.; Vanmaekelbergh, D. Lasing Supraparticles Self-Assembled from Nanocrystals. *ACS Nano* **2018**, *12*, 12788−12794.
(5) Wang, K.; Sun, W.; Li, J.; Gu, Z.; Xiao, S.; Song, Q. Unidirectional Lasing Emissions from $CH_3NH_3PbBr_3$ Perovskite Microdisks. *ACS Photonics* **2016**, *3*, 1125−1130.
(6) Chen, Y.; Ryou, A.; Friedfeld, M. R.; Fryett, T.; Whitehead, J.; Cossairt, B. M.; Majumdar, A. Deterministic Positioning of Colloidal Quantum Dots on Silicon Nitride Nanobeam Cavities. *Nano Lett.* **2018**, *18*, 6404−6410.
(7) Fong, C. F.; Yin, Y.; Chen, Y.; Rosser, D.; Xing, J.; Majumdar, A.; Xiong, Q. Silicon nitride nanobeam enhanced emission from all-inorganic perovskite nanocrystals. *Opt. Express* **2019**, *27*, 18673.
(8) Yang, Z.; Pelton, M.; Fedin, I.; Talapin, D. V.; Waks, E. A room temperature continuous-wave nanolaser using colloidal quantum wells. *Nat. Commun.* **2017**, *8*, No. 143.
(9) Grim, J. Q.; Christodoulou, S.; Di Stasio, F.; Krahne, R.; Cingolani, R.; Manna, L.; Moreels, I. Continuous-wave biexciton lasing at room temperature using solution-processed quantum wells. *Nat. Nanotechnol.* **2014**, *9*, 891−895.
(10) Flatten, L. C.; Christodoulou, S.; Patel, R. K.; Buccheri, A.; Coles, D. M.; Reid, B. P. L.; Taylor, R. A.; Moreels, I.; Smith, J. M. Strong Exciton−Photon Coupling with Colloidal Nanoplatelets in an Open Microcavity. *Nano Lett.* **2016**, *16*, 7137−7141.
(11) Baghani, E.; O'Leary, S. K.; Fedin, I.; Talapin, D. V.; Pelton, M. Auger-Limited Carrier Recombination and Relaxation in CdSe Colloidal Quantum Wells. *J. Phys. Chem. Lett.* **2015**, *6*, 1032−1036.
(12) Pelton, M. Carrier Dynamics, Optical Gain, and Lasing with Colloidal Quantum Wells. *J. Phys. Chem. C* **2018**, *122*, 10659−10674.
(13) He, Z.; Chen, B.; Hua, Y.; Liu, Z.; Wei, Y.; Liu, S.; Hu, A.; Shen, X.; Zhang, Y.; Gao, Y.; Liu, J. CMOS Compatible High-Performance Nanolasing Based on Perovskite−SiN Hybrid Integration. *Adv. Opt. Mater.* **2020**, *8*, No. 2000453.
(14) She, C.; Fedin, I.; Dolzhnikov, D. S.; Dahlberg, P. D.; Engel, G. S.; Schaller, R. D.; Talapin, D. V. Red, Yellow, Green, and Blue Amplified Spontaneous Emission and Lasing Using Colloidal CdSe Nanoplatelets. *ACS Nano* **2015**, *9*, 9475−9485.
(15) Hazarika, A.; Fedin, I.; Hong, L.; Guo, J.; Srivastava, V.; Cho, W.; Coropceanu, I.; Portner, J.; Diroll, B. T.; Philbin, J. P.; et al. Colloidal Atomic Layer Deposition with Stationary Reactant Phases Enables Precise Synthesis of "Digital" II−VI Nano-heterostructures with Exquisite Control of Confinement and Strain. *J. Am. Chem. Soc.* **2019**, *141*, 13487−13496.
(16) Beadie, G.; Brindza, M.; Flynn, R. A.; Rosenberg, A.; Shirk, J. S. Refractive index measurements of poly(methyl methacrylate) (PMMA) from 04−16 μm. *Appl. Opt.* **2015**, *54*, F139.
(17) Fryett, T. K.; Chen, Y.; Whitehead, J.; Peycke, Z. M.; Xu, X.; Majumdar, A. Encapsulated Silicon Nitride Nanobeam Cavity for Hybrid Nanophotonics. *ACS Photonics* **2018**, *5*, 2176−2181.
(18) Cohen, T. A.; Sharp, D.; Kluherz, K. T.; Chen, Y.; Munley, C.; Anderson, R. T.; Swanson, C. J.; De Yoreo, J. J.; Luscombe, C. K.; Majumdar, A.; et al. Direct Patterning of Perovskite Nanocrystals on Nanophotonic Cavities with Electrohydrodynamic Inkjet Printing. *Nano Lett.* **2022**, *22*, 5681−5688.
(19) Meldrum, A.; Bianucci, P.; Marsiglio, F. Modification of ensemble emission rates and luminescence spectra for inhomogeneously broadened distributions of quantum dots coupled to optical microcavities. *Opt. Express* **2010**, *18*, 10230.
(20) Kunneman, L. T.; Schins, J. M.; Pedetti, S.; Heuclin, H.; Grozema, F. C.; Houtepen, A. J.; Dubertret, B.; Siebbeles, L. D. A. Nature and Decay Pathways of Photoexcited States in CdSe and CdSe/CdS Nanoplatelets. *Nano Lett.* **2014**, *14*, 7039−7045.
(21) Wu, S.; Buckley, S.; Schaibley, J. R.; Feng, L.; Yan, J.; Mandrus, D. G.; Hatami, F.; Yao, W.; Vučković, J.; Majumdar, A.; Xu, X. Monolayer semiconductor nanocavity lasers with ultralow thresholds. *Nature* **2015**, *520*, 69−72.
(22) Bjork, G.; Yamamoto, Y. Analysis of semiconductor microcavity lasers using rate equations. *IEEE J. Quantum Electron.* **1991**, *27*, 2386−2396.
(23) Cho, W.; Kim, S.; Coropceanu, I.; Srivastava, V.; Diroll, B. T.; Hazarika, A.; Fedin, I.; Galli, G.; Schaller, R. D.; Talapin, D. V. Direct Synthesis of Six-Monolayer (1.9 nm) Thick Zinc-Blende CdSe Nanoplatelets Emitting at 585 nm. *Chem. Mater.* **2018**, *30*, 6957−6960.
(24) Hinterding, S. O. M.; Salzmann, B. B. V.; Vonk, S. J. W.; Vanmaekelbergh, D.; Weckhuysen, B. M.; Hutter, E. M.; Rabouw, F. T. Single Trap States in Single CdSe Nanoplatelets. *ACS Nano* **2021**, *15*, 7216−7225.
(25) Rodà, C.; Di Giacomo, A.; Tasende Rodríguez, L. C.; M, C. S.; Leemans, J.; Hens, Z.; Geiregat, P.; Moreels, I. Colloidal CdSe/CdS Core/Crown Nanoplatelets for Efficient Blue Light Emission and Optical Amplification. *Nano Lett.* **2023**, *23*, 3224−3230.
(26) Erdem, O.; Foroutan, S.; Gheshlaghi, N.; Guzelturk, B.; Altintas, Y.; Demir, H. V. Thickness-Tunable Self-Assembled Colloidal Nanoplatelet Films Enable Ultrathin Optical Gain Media. *Nano Lett.* **2020**, *20*, 6459−6465.
(27) Shin, A. J.; Hossain, A. A.; Tenney, S. M.; Tan, X.; Tan, L. A.; Foley, J. J.; Atallah, T. L.; Caram, J. R. Dielectric Screening Modulates Semiconductor Nanoplatelet Excitons. *J. Phys. Chem. Lett.* **2021**, *12*, 4958−4964.
(28) Björk, G.; Karlsson, A.; Yamamoto, Y. On the linewidth of microcavity lasers. *Appl. Phys. Lett.* **1992**, *60*, 304−306.
(29) Kang, H.; Ma, J.; Li, J.; Zhang, X.; Liu, X. Exciton Polaritons in Emergent Two-Dimensional Semiconductors. *ACS Nano* **2023**, *17*, 24449−24467.
(30) Jo, K.; Marino, E.; Lynch, J.; Jiang, Z.; Gogotsi, N.; Darlington, T. P.; Soroush, M.; Schuck, P. J.; Borys, N. J.; Murray, C. B.; Jariwala, D. Direct nano-imaging of light-matter interactions in nanoscale excitonic emitters. *Nat. Commun.* **2023**, *14*, No. 2649.
(31) Zhang, Q.; Zhu, Y.; Niu, P.; Lao, C.; Yao, Y.; Liu, W.; Yang, Q. F.; Chu, S.; Gao, Y. Low-Threshold Single-Mode Microlasers from Green CdSe/CdSeS Core/Alloyed-Crown Nanoplatelets. *ACS Photonics* **2023**, *10*, 1397−1404.
(32) Hodaei, H.; Miri, M. A.; Hassan, A. U.; Hayenga, W. E.; Heinrich, M.; Christodoulides, D. N.; Khajavikhan, M. Parity-time-symmetric coupled microring lasers operating around an exceptional point. *Opt. Lett.* **2015**, *40*, 4955.
(33) Ahn, N.; Livache, C.; Pinchetti, V.; Jung, H.; Jin, H.; Hahm, D.; Park, Y. S.; Klimov, V. I. Electrically driven amplified spontaneous emission from colloidal quantum dots. *Nature* **2023**, *617*, 79−85.

https://doi.org/10.1021/acsphotonics.4c00377
ACS Photonics XXXX, XXX, XXX−XXX